

# A new probe of magnetic fields in the pre-reionization epoch: II. Detectability

Vera Gluscevic,<sup>1</sup> Tejaswi Venumadhav,<sup>1</sup> Abhilash Mishra,<sup>2</sup> Antonija Oklopcic,<sup>2</sup> and Christopher Hirata<sup>3</sup>

<sup>1</sup>*Institute for Advanced Study, Einstein Drive, Princeton, NJ 08540, USA*

<sup>2</sup>*California Institute of Technology, Mail Code 350-17, Pasadena, CA 91125, USA*

<sup>3</sup>*Center for Cosmology and Astroparticle Physics, The Ohio State University,*

*191 West Woodruff Lane, Columbus, Ohio 43210, USA*

(Dated: December 8, 2015)

In the first paper of this series, we proposed a novel method to detect large-scale magnetic fields in the Dark Ages, using 21-cm tomography surveys. In this paper, we examine detectability of magnetic fields using this method. We first develop a minimum-variance estimator formalism to measure magnetif fields using the characteristic anisotropic imprints in the 21-cm brightness-temperature 2-point correlation functions. We then evaluate Fisher expressions for this estimator and find that a radio array presenting about a square kilometer of area covered in dipole antennas (such as the next-generation of HERA, or the SKA in a tightly-packed configuration) can detect fields of strength on the order of  $10^{-21}$  Gauss (scaled to present day)—almost 10 orders of magnitude below the CMB constraints. Measurement of the field strength will, however, require more futuristic arrays.

## I. INTRODUCTION

Magnetic fields are ubiquitous in the universe on all observed scales [1–5]. However, the origins of the magnetic fields in Galaxies and on large scales are as of yet an unresolved question. Various forms of dynamo mechanisms [6] are proposed to maintain and amplify magnetic fields, but they typically require seed fields to act [1]. The seed fields may be produced during structure formation through Biermann battery or similar mechanisms [7, 8], or otherwise may be relics from the early universe [1, 9, 10]. Observations of large-scale weak magnetic fields in the high-redshift intergalactic medium (IGM) can thus provide tools for understanding the origins of magnetic fields in the present-day universe, and potentially open up an entirely new window into the physics of the early universe.

Many observational probes have previously been used to search for evidence of large-scale magnetic fields locally and at high redshifts; see, e. g. [4, 11–19]. Amongst the most sensitive tracers of cosmological magnetic fields are the measurements of the cumulative effect of Faraday rotation in the cosmic-microwave-background polarization maps, which currently place an upper limit of  $\sim 10^{-10}$  Gauss (in comoving units) using the data from the Planck satellite [20]. In Paper I of this series [21], we proposed a novel method to detect and measure extremely weak cosmological magnetic fields during the pre-reionization epoch (the Dark Ages). This method relies on future 21-cm brightness-temperature tomography surveys [22, 23], many of which have pathfinder experiments currently running [24–29], and plans for the next stages to be realized in the coming decade [27, 29]. As we show in Paper I, the measurement of statistical anisotropy in the 21-cm signal from the Dark Ages has intrinsic sensitivity to magnetic fields in the IGM more than *10 orders of magnitude below the current upper limits*.

While Paper I laid out the formalism necessary to account for the effect of magnetic fields on the statistics of the 21-cm signal, this paper (which we refer to as

Paper II in the following) focuses on evaluating the sensitivity of future 21-cm experiments using this method. The rest of this paper is organized as follows. In §II, we present a quick overview of the main results in Paper I. In §IV, we derive minimum-variance estimators for a uniform and stochastic magnetic field. In §V, we set up the Fisher analysis formalism necessary to evaluate detectability. In §VI, we present numerical results, and we conclude in §VII. Supporting materials are presented in the appendices.

## II. SUMMARY OF THE METHOD

Magnetic moments of hydrogen atoms in the excited state of the 21-cm line transition tend to be aligned with the incident quadrupole of the 21-cm radiation from the surrounding medium. This effect of “ground-state alignment” [30, 31] arises in a cosmological setting due to velocity-field gradients. In the presence of external large-scale magnetic fields, the emitted 21-cm quadrupole is misaligned with the incident quadrupole, due to atomic precession (illustrated in Figure 1). The resulting emission anisotropy can thus be used to trace magnetic fields at high redshifts.

The main result of Paper I was a calculation of the 21-cm brightness temperature  $T_b$  as a function of the line of sight (LOS) direction  $\hat{\mathbf{n}}$ , in the frame of the emitting ensemble of atoms. The relevant expression is

$$\begin{aligned} \delta T_b(\hat{\mathbf{n}}) = & \left(1 - \frac{T_\gamma}{T_s}\right) x_{1s} \left(\frac{1+z}{10}\right)^{1/2} \\ & \times \left[ 26.4 \text{ mK} \left\{ 1 + \left(1 + (\hat{\mathbf{k}} \cdot \hat{\mathbf{n}})^2\right) \delta \right\} - 0.128 \text{ mK} \left(\frac{T_\gamma}{T_s}\right) \right. \\ & \times x_{1s} \left(\frac{1+z}{10}\right)^{1/2} \left\{ 1 + 2 \left(1 + (\hat{\mathbf{k}} \cdot \hat{\mathbf{n}})^2\right) \delta \right. \\ & \left. \left. - \frac{\delta}{15} \sum_m \frac{4\pi}{5} \frac{Y_{2m}(\hat{\mathbf{k}}) [Y_{2m}(\hat{\mathbf{n}})]^*}{1 + x_{\alpha,(2)} + x_{c,(2)} - imx_B} \right\} \right], \end{aligned} \quad (1)$$

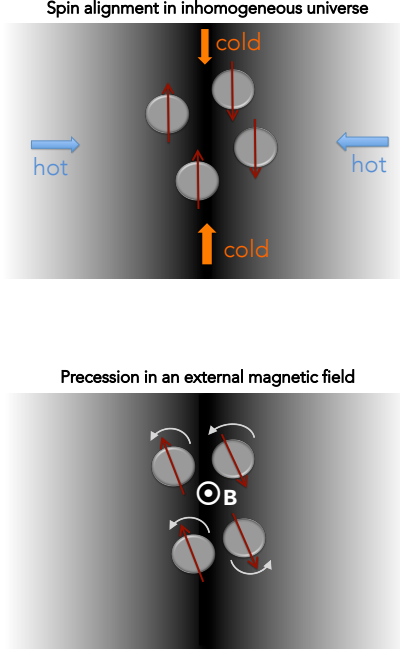


Figure 1. Illustration of the effect of a magnetic field on hydrogen atoms in the excited state of 21-cm transition at high redshifts. In the classical picture, magnetic moments of the atoms (depicted as red arrows) tend to be aligned with density gradients (upper panel; the gradient is depicted with the background shading), unless they precess about the direction of ambient magnetic field (pointing out of the page on the lower panel). When the precessing atoms decay back into the ground state, the emitted quadrupole (aligned with the direction of the magnetic moments) is misaligned with the incident quadrupole. This offset can be observed as a statistical anisotropy of 21-cm-brightness-temperature correlation functions, and used to trace cosmological magnetic fields.

where  $x_{\alpha,(2)}$ ,  $x_{c,(2)}$  and  $x_B$  parametrize the rates of depolarization of the ground state by optical pumping, collisions, and magnetic precession (relative to radiative depolarization), respectively (defined in detail in Paper I). Furthermore,  $T_s$  and  $T_\gamma$  are the spin temperature and the temperature of the cosmic microwave background at redshift  $z$ , respectively;  $\hat{\mathbf{k}}$  is a unit vector in the direction of the wave-vector  $\vec{k}$  of a given density Fourier mode; and  $Y_{2m}$  represent the usual spin-zero spherical harmonics. Figure 2 illustrates the effect of the magnetic field on the brightness temperature emission pattern in the frame of the atom; shown are quadrupole patterns corresponding to the sum-term of Eq. (1), for various strengths of the magnetic field. Notice that there is a saturation limit for the field strength—for strong enough fields, the precession time is much smaller than the lifetime in the excited state, and when the emission pattern asymptotes to the one shown in the bottom panel of Figure 2. Above this limit, approximation of linear dependence of  $T_b$  breaks

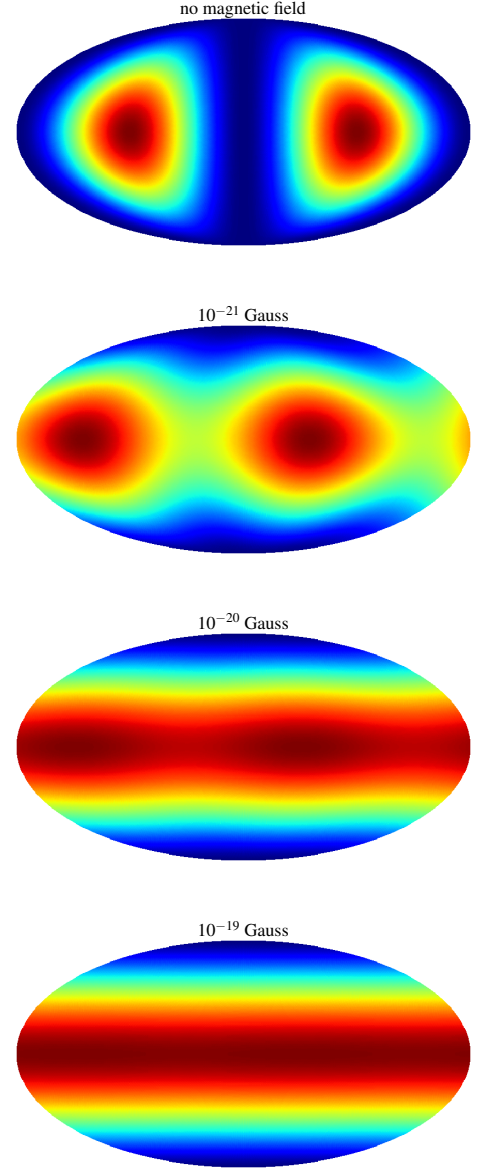


Figure 2. Illustration of the quadrupolar pattern of 21-cm emission from the last ( $B$ -dependent) term of Eq. (1) in the frame of the emitting atoms, for the case where  $\vec{k}$  is perpendicular to  $\hat{\mathbf{n}}$  (maximal signal), shown in Mollweide projection. Lower panels correspond to increasingly stronger magnetic fields (strength denoted on each panel in comoving units), with the bottom panel corresponding to the saturated case. Notice how the type of quadrupole differs for the no-magnetic field case and the case the field is “strong” in the saturation sense.

down, which implies that the signal cannot be used to reconstruct the strength of the field; however, it is still possible to distinguish saturated regime from the case of null field, as we will see in §V.

The affect of quadrupole misalignment arises at second order in optical depth (it is a result of a two-

scattering process), and is thus a small correction to the total brightness temperature. However, owing to the long lifetime of the excited state (during which even an extremely slow precession has large cumulative effect on the direction of the quadrupole at second order), the effect of misalignment is exclusively sensitive to magnetic fields in the IGM at redshifts prior to cosmic reionization—as we show in Paper I, a miniscule magnetic field strength of  $10^{-21}$  Gauss (in comoving units) produces order-one changes in the direction of the quadrupole. This means that a high-precision measurement of the 21-cm brightness-temperature 2-point correlation function intrinsically has that level of sensitivity to detecting magnetic fields in the Dark Ages. We now proceed to develop a formalism to search for this effect, with future surveys of redshifted 21-cm line, and to identifying experimental setups that can reach it.

### III. BASICS

Before focusing on the estimator formalism in the next Section, here we review the basics of 21-cm brightness temperature fluctuation measurements. In §III A, we review definitions of quantities describing sensitivity of interferometric radio arrays; in §III B, we focus on the derivation of the noise power spectrum; and in §III C, we discuss the effects of the array configuration and its relation to coverage of modes in the  $uv$  plane of the array.

#### A. Definitions

The redshifted 21-cm signal can be represented as a specific intensity at the location in physical space  $I(\vec{r})$ , or in Fourier space  $\tilde{I}(\vec{k})$ . In sky coordinates (centered on an emitting patch of the sky), these functions become  $\mathcal{I}(\theta_x, \theta_y, \theta_\nu)$ , and  $\tilde{\mathcal{I}}(u, v, \eta)$ , respectively. Here, vector  $\vec{k}$  (in the units of comoving  $\text{Mpc}^{-1}$ ) is a Fourier dual of  $\vec{r}$  (comoving Mpc), and likewise,  $\theta_x$  (rad),  $\theta_y$  (rad), and  $\theta_\nu$  (Hz) are duals of the coordinates  $u$  ( $\text{rad}^{-1}$ ),  $v$  ( $\text{rad}^{-1}$ ), and  $\eta$  (seconds), respectively. Notice that  $\theta_x$  and  $\theta_y$  represent the angular extent of the patch in the sky, while  $\theta_\nu$  represents its extent in the frequency space. The two sets of coordinates are related through linear transformations in the following way

$$\begin{aligned} \theta_x &= \frac{r_x}{\chi(z)}, & u &= \frac{k_x \chi(z)}{2\pi}, \\ \theta_y &= \frac{r_y}{\chi(z)}, & v &= \frac{k_y \chi(z)}{2\pi}, \\ \theta_\nu &= \frac{H(z)\nu_{21}}{c(1+z)^2} r_z, & \eta &= \frac{c(1+z)^2}{2\pi H(z)\nu_{21}} k_z, \end{aligned} \quad (2)$$

where  $\nu_{21}$  is the 21-cm frequency in the rest frame of emitting atoms,  $H(z)$  is the Hubble parameter,  $\chi(z)$  is the comoving distance to redshift  $z$ , which marks the

middle of the observed data cube (where  $r_z$  and  $\theta_\nu$  intervals are evaluated). Note that conditions of the type  $2\pi\theta_x u = r_x k_x$  are satisfied.

The convention we use for the Fourier transforms is (note that Fourier-space functions are denoted with tilde)

$$\begin{aligned} I(\vec{r}) &= \int \tilde{I}(\vec{k}) e^{i\vec{k}\cdot\vec{r}} d^3\vec{k}, \\ \tilde{I}(\vec{k}) &= \frac{1}{(2\pi)^3} \int I(\vec{r}) e^{-i\vec{k}\cdot\vec{r}} d^3\vec{r}, \end{aligned} \quad (3)$$

and similarly,

$$\begin{aligned} \mathcal{I}(\theta_x, \theta_y, \theta_\nu) &= \int \tilde{\mathcal{I}}(u, v, \eta) e^{2\pi i(u\theta_x + v\theta_y + \eta\theta_\nu)} du dv d\eta, \\ \tilde{\mathcal{I}}(u, v, \eta) &= \int \mathcal{I}(\theta_x, \theta_y, \theta_\nu) e^{-2\pi i(u\theta_x + v\theta_y + \eta\theta_\nu)} d\theta_x d\theta_y d\theta_\nu. \end{aligned} \quad (4)$$

The following scaling relation is satisfied

$$\tilde{I}(\vec{k}) = \frac{c(1+z)^2 \chi(z)^2}{(2\pi)^3 H(z) \nu_{21}} \tilde{\mathcal{I}}(u, v, \eta), \quad (5)$$

where the proportionality factor contains a Jacobian  $\frac{dr_x dr_y dr_z}{d\theta_x d\theta_y d\theta_\nu}$ . Finally, the relationship between the specific intensity in the  $uv$ -plane and the visibility function  $V(u, v, \theta_\nu)$  is given by a Fourier transform over only the frequency coordinate,

$$\begin{aligned} V(u, v, \theta_\nu) &= \int \tilde{\mathcal{I}}(u, v, \eta) e^{2\pi i \theta_\nu \eta} d\eta, \\ \tilde{\mathcal{I}}(u, v, \eta) &= \int V(u, v, \theta_\nu) e^{-2\pi i \theta_\nu \eta} d\theta_\nu, \end{aligned} \quad (6)$$

Here,  $\theta_{\nu, \text{max}} - \theta_{\nu, \text{min}} = \Delta\nu$  is the bandwidth of the observed data cube centered on  $z$  (see also Appendix A).

#### B. Power spectra and noise

In this Section, we derive the noise power spectrum for the brightness temperature signal. We start by defining a brightness-temperature power spectrum as

$$\langle \tilde{I}(\vec{k}) \tilde{I}^*(\vec{k}') \rangle \equiv (2\pi)^3 P_I \delta_D(\vec{k} - \vec{k}'), \quad (7)$$

where  $\delta_D$  is the Dirac delta function. The observable we wish to relate this power spectrum to is the visibility function—a complex Gaussian variable with a zero mean, whose noise-induced variance (derived in Appendix A) reads

$$\begin{aligned} &\langle V(u, v, \theta_\nu) V(u', v', \theta'_\nu)^* \rangle \\ &= \left( \frac{2k_B T_{\text{sky}}}{A_e \sqrt{\Delta\nu t_1}} \right)^2 \delta_D(u - u') \delta_D(v - v') \delta_{\theta_\nu \theta'_\nu}, \end{aligned} \quad (8)$$

where  $T_{\text{sky}}$  is the sky temperature;  $t_1$  is the total time a single baseline spent observing an element at the position  $(u, v)$  in the  $uv$  plane;  $A_e$  is the collecting area of a single

dish;  $k_B$  is Boltzmann constant;  $\Delta\nu$  is the bandwidth centered on  $z$ ; and  $\delta$  symbol with subscripts denotes the Kronecker delta.

The next step is to combine Eqs. (6) and (8), and take ensemble average to get

$$\begin{aligned} & \langle \tilde{\mathcal{I}}(u, v, \eta) \tilde{\mathcal{I}}^*(u', v', \eta') \rangle \\ &= \frac{1}{t_1} \left( \frac{2k_B T_{\text{sys}}}{A_e} \right)^2 \delta_D(u - u') \delta_D(v - v') \delta(\eta - \eta'), \end{aligned} \quad (9)$$

where

$$\int e^{2\pi i \theta_\nu (\eta - \eta')} d\theta_\nu = \delta_D(\eta - \eta'), \quad (10)$$

is the periodic delta-function on the  $t_1$  interval. Taking into account the scaling relation of Eq. (5), introducing the power spectrum of Eq. (7), and keeping in mind the scaling property of the delta function, we arrive at

$$P_1^N(\vec{k}) = \frac{1}{t_1 (2\pi)^6} \frac{c(1+z)^2 \chi^2(z)}{H(z) \nu_{21}} \left( \frac{2k_B T_{\text{sky}}}{A_e} \right)^2, \quad (11)$$

for the noise per  $\vec{k}$  mode, per baseline.

Computation of  $t_1$  from the total duration of the survey  $t_{\text{obs}}$  depends on the type of the experiment. For a beam of a solid angle  $\Omega_{\text{beam}} = \lambda^2/A_e$  much smaller than the solid angle of the entire survey,  $\Omega_{\text{survey}}$ , where telescopes scan the sky one beamwidth at a time (such as the case for radio dishes),  $t_1$  is the total time spent observing one  $uv$  element of size corresponding to the beam size,  $t_1 = t_{\text{obs}} \Omega_{\text{survey}}/\Omega_{\text{beam}}$ . However, in the case of an array of dipoles, the beam is greater or equal to the survey angular size, and  $t_1 = t_{\text{obs}}$ . When deriving numerical results in §VI, we will assume the latter. Finally, we will not account for the fact that a given patch of the sky is only visible for a part of a day from a given location; therefore,  $t_{\text{obs}}$  we use in §VI is the survey duration times a factor of a few or less that corrects for this assumption.

The last step is to get from Eq. (11) to the expression for the noise power spectrum that corresponds to the observation with all the available baselines. To do that, we need to incorporate the knowledge about the array configuration and the coverage of the  $uv$  plane. In other words, we need to divide the expression in Eq. (11) by the number of baselines that see a given mode  $\vec{k}$  at any given time  $n_{\text{base}}(\vec{k})$  (for a discussion of the  $uv$  coverage, see the following section). The final result for the noise power spectrum per mode  $\vec{k}$  in the intensity units is then

$$P^N(\vec{k}) = \frac{1}{t_1 (2\pi)^6} \frac{c(1+z)^2 \chi^2(z)}{H(z) \nu_{21}} \frac{(2k_B T_{\text{sys}})^2}{A_e^2 n_{\text{base}}(\vec{k})}, \quad (12)$$

and in temperature units

$$P^N(\vec{k}) = \frac{\lambda^4}{t_1 (2\pi)^6} \frac{c(1+z)^2 \chi^2(z)}{H(z) \nu_{21}} \frac{T_{\text{sys}}^2}{A_e^2 n_{\text{base}}(\vec{k})}. \quad (13)$$

### C. The UV coverage

Total number density  $n_{\text{base}}(\vec{k})$  of baselines that can observe mode  $\vec{k}$  is related to the (unitless) number density  $n(u, v)$  of baselines per  $dudv$  element as

$$n_{\text{base}}(\vec{k}) = \frac{n(u, v)}{\Omega_{\text{beam}}}, \quad (14)$$

where  $\frac{1}{\Omega_{\text{beam}}}$  represents an element in the  $uv$  plane. The number density integrates to the total number of baselines  $N_{\text{base}}$ ,

$$N_{\text{base}} = \frac{1}{2} N_{\text{ant}} (N_{\text{ant}} + 1) = \int_{\text{half}} n(u, v) dudv, \quad (15)$$

where  $N_{\text{ant}}$  is the number of antennas in the array, and the integration is done on the half of the  $uv$  plane (because the visibility has the following property  $V(u, v, \theta_\nu) = V^*(-u, -v, \theta_\nu)$ , and only half the plane contains independent samples). We assume that the array consists of many antennas, so that time-dependence of  $n(u, v)$  is negligible; if this is not the case, one should compute its time average to account for Earth's rotation.

Let us now consider  $n_{\text{base}}(\vec{k})$  for a specific array configuration that is of particular interest to cosmology—a tightly packed array of simple dipole antennas, tiling a squared-surface of the area  $(\Delta L)^2$  with a filling fraction close to one. This is a design such as the Fast Fourier Transform Telescope (FFTT) described in [32]. In this case, the beam solid angle is 1 sr, the effective area of a single dipole is  $A_e = \lambda^2$ , and the effective number of antennas is then  $N_{\text{ant}} = \frac{(\Delta L)^2}{\lambda^2}$ . For such configuration

$$n(u, v) = \left( \frac{\Delta L}{\lambda} - u \right) \left( \frac{\Delta L}{\lambda} - v \right). \quad (16)$$

The relation between  $\vec{k} = (k, \theta_k, \phi_k)$  and  $(u, v)$  is

$$\begin{aligned} u_\perp &\equiv \frac{D_A(z)}{2\pi} k \sin \theta_k, \\ u &= u_\perp \cos \phi_k, \\ v &= u_\perp \sin \phi_k, \end{aligned} \quad (17)$$

where subscript  $\perp$  denotes components perpendicular to the LOS direction  $\hat{\mathbf{n}}$ , and  $D_A$  is the angular diameter distance. From this, the corresponding number of baselines observing a given  $\vec{k}$  is

$$\begin{aligned} n_{\text{base}}(\vec{k}) &= \left( \frac{\Delta L}{\lambda} - \frac{D_A(z)}{2\pi} k \sin \theta_k \cos \phi_k \right) \\ &\times \left( \frac{\Delta L}{\lambda} - \frac{D_A(z)}{2\pi} k \sin \theta_k \sin \phi_k \right). \end{aligned} \quad (18)$$

In §VI, we use a  $\phi_k$ -averaged version of this quantity (between 0 and  $\pi/2$  only, due to the four-fold symmetry of the experimental setup of a square of dipoles), to account for the rotation of the baselines with respect to the

modes,

$$\langle n_{\text{base}}(\vec{k}) \rangle_{\phi_k} = \left( \frac{\Delta L}{\lambda} \right)^2 - \frac{4}{\pi} \frac{\Delta L}{\lambda} \frac{D_A(z)}{2\pi} k \sin \theta_k + \left( \frac{D_A(z)}{2\pi} k \sin \theta_k \right)^2. \quad (19)$$

#### IV. QUADRATIC ESTIMATOR FORMALISM

We now derive an unbiased minimum-variance quadratic estimator for a cosmic magnetic field  $\vec{B}$ , following a formalism similar to what is used in CMB studies [33]. We first assume that the field is uniform across the survey volume, and only evolves with redshift due to the expansion of the universe as

$$B(z) = B_0(1+z)^2, \quad (20)$$

where  $B_0$  represents its present-day value (or equivalently, its value in comoving units); the relevant estimator is denoted by a hat sign,  $\hat{B}_0$ . Then we move on to the case of a stochastic magnetic field, with a given power spectrum  $P_B(\vec{K})$  where  $\vec{K}$  denotes the wavevector for the mode of the field; in this case, the relevant estimator is of its amplitude,  $\hat{A}_0$ . In both cases, the presented formalism is only valid if there the following separation of scales is satisfied: density-field modes in consideration must have much smaller wavelengths than the coherence scale of the magnetic field (or a given mode of a stochastic magnetic field), and both must be smaller than the size of the tomography survey at hand.

##### A. Uniform field

We first derive an unbiased minimum-variance quadratic estimator  $\hat{B}_0$  for a comoving uniform magnetic field. We start by noting that the redshifted 21-cm brightness temperature Fourier modes  $T(\vec{k})$  contain contribution from the noise  $T^N(\vec{k})$  and the signal  $T^S(\vec{k})$ , where the signal contains contributions from the 21-cm signal with no magnetic field (null-case signal  $T_0^S(\vec{k})$ ), and with the magnetic field,

$$\begin{aligned} T(\vec{k}) &= T^N(\vec{k}) + T^S(\vec{k}), \\ T^S(\vec{k}) &= T_0^S(\vec{k}) + B_0 \frac{\partial T_0^S}{\partial B_0}(\vec{k}), \end{aligned} \quad (21)$$

where  $B$  is a small expansion parameter (we adopt the linear-theory approach through this work). We use the subscript “0” to denote functions evaluated at  $B = 0$ . Temperature is proportional to the density fluctuation  $\delta$ , with the transfer function  $G(\hat{\mathbf{k}})$  as the proportionality factor,

$$\begin{aligned} T^S(\vec{k}) &= G(\hat{\mathbf{k}})\delta(k), \\ T_0^S(\vec{k}) &= G_0(\hat{\mathbf{k}})\delta(k), \end{aligned} \quad (22)$$

where  $\hat{\mathbf{k}} = (\theta_k, \phi_k)$  is a unit vector in the direction of  $\vec{k}$ . Note that while  $G$  is a function of the direction vector

$\hat{\mathbf{k}}$  only, the power spectrum  $P_\delta$  is a function of the magnitude  $k$ , in an isotropic universe. For simplicity of the expressions, we adopt the following notation

$$\begin{aligned} \frac{\partial T_0^S}{\partial B}(\vec{k}) &\equiv \delta(k) \frac{\partial G}{\partial B_0}(\hat{\mathbf{k}}, B_0 = 0), \\ \frac{\partial G_0}{\partial B}(\hat{\mathbf{k}}) &\equiv \frac{\partial G}{\partial B_0}(\hat{\mathbf{k}}, B_0 = 0) \end{aligned} \quad (23)$$

Furthermore, we denote the power spectrum in the null case as

$$P_{\text{null}}(\vec{k}) \equiv P^N(\vec{k}) + P_0^S(\vec{k}). \quad (24)$$

The signal power spectrum in the absence of a magnetic field is given as

$$\begin{aligned} \langle T_0(\vec{k}) T_0^*(\vec{k}') \rangle &\equiv (2\pi)^3 \delta_D(\vec{k} - \vec{k}') P_0^S(\vec{k}) \\ &= (2\pi)^3 \delta_D(\vec{k} - \vec{k}') G_0^2(\hat{\mathbf{k}}) P_\delta(k), \end{aligned} \quad (25)$$

where

$$\langle \delta(\vec{k}) \delta^*(\vec{k}') \rangle \equiv (2\pi)^3 \delta_D(\vec{k} - \vec{k}') P_\delta(k). \quad (26)$$

The observable 2-point correlation function in Fourier space is

$$\begin{aligned} \langle T(\vec{k}) T^*(\vec{k}') \rangle &= P_{\text{null}}(\vec{k}) (2\pi)^3 \delta_D(\vec{k} - \vec{k}') \\ &+ \langle T_0^S(\vec{k}) B_0 \frac{\partial T_0^{S,*}}{\partial B}(\vec{k}') \rangle + \langle T_0^{S,*}(\vec{k}') B_0 \frac{\partial T_0^S}{\partial B}(\vec{k}) \rangle \\ &= \left( P_{\text{null}}(\vec{k}) + 2B_0 P_\delta(k) \text{Re} \left[ G_0^*(\hat{\mathbf{k}}) \frac{\partial G_0}{\partial B}(\hat{\mathbf{k}}) \right] \right) \\ &\quad \times (2\pi)^3 \delta_D(\vec{k} - \vec{k}'), \end{aligned} \quad (27)$$

where we assume that the signal and the noise are uncorrelated and keep only terms linear in  $B_0$ .

Since we observe only one universe, the measured proxy for the ensemble average in Eq. (27) is the product  $T(\vec{k}) T^*(\vec{k}')$ . Using Eq. (27), each  $T(\vec{k})$  gives an estimate for  $B_0$ ,

$$\hat{B}_0^{\vec{k}} = \frac{\frac{1}{V} T(\vec{k}) T^*(\vec{k}) - P_{\text{null}}(\vec{k})}{2P_\delta(\vec{k}) \text{Re} \left[ G_0(\hat{\mathbf{k}}) \frac{\partial G_0}{\partial B}(\hat{\mathbf{k}}) \right]}, \quad (28)$$

where we use the reality of  $G$  in the null case and the following property of the Dirac delta function on a finite volume of the survey  $V$

$$\delta_D(\vec{k} - \vec{k}') = \frac{V}{(2\pi)^3}, \quad \text{for } \vec{k} = \vec{k}', \quad (29)$$

related to the Kronecker delta as

$$\delta_{\vec{k}\vec{k}'} = \frac{(2\pi)^3}{V} \delta_D(\vec{k} - \vec{k}'). \quad (30)$$

The estimator of Eq. (28) is unbiased,  $\langle \hat{B}_0^{\vec{k}} \rangle = 0$ . The covariance of the estimates from all available modes is given by

$$\langle \widehat{B}_0^{\vec{k}} \widehat{B}_0^{\vec{k}',*} \rangle = \frac{\left\langle \left( \frac{1}{V} T(\vec{k}) T^*(\vec{k}) - P_{\text{null}}(\vec{k}) \right) \left( \frac{1}{V} T^*(\vec{k}') T(\vec{k}') - P_{\text{null}}(\vec{k}') \right) \right\rangle}{4P_\delta(k)P_\delta(k') \text{Re} \left[ G_0(\widehat{\mathbf{k}}) \frac{\partial G_0}{\partial B}(\widehat{\mathbf{k}}) \right] \text{Re} \left[ G_0(\widehat{\mathbf{k}}') \frac{\partial G_0}{\partial B}(\widehat{\mathbf{k}}') \right]}, \quad (31)$$

The expectation value in the above equation involves temperature-field 4-point correlation. If we enumerate factors of “ $T$ ” in this correlation as  $\langle 1 \ 2 \ 3 \ 4 \rangle$ , the 4-point function is a sum of the following contractions (assuming Gaussianity of the temperature field in the null case):  $\langle T(\vec{k}) T^*(\vec{k}) T^*(\vec{k}') T(\vec{k}') \rangle = \langle 1 \ 2 \rangle \langle 3 \ 4 \rangle + \langle 1 \ 4 \rangle \langle 2 \ 3 \rangle + \langle 1 \ 3 \rangle \langle 2 \ 4 \rangle$ . Keeping this order of summands,

$$\begin{aligned} & \langle T(\vec{k}) T^*(\vec{k}) T^*(\vec{k}') T(\vec{k}') \rangle \\ &= V^2 P_{\text{null}}(\vec{k}) P_{\text{null}}(\vec{k}') \left( 1 + \delta_{\vec{k}, \vec{k}'} + \delta_{\vec{k}, -\vec{k}'} \right) \end{aligned} \quad (32)$$

where we used Eqs. (29) and (30). The rest of the terms in Eq. (31) are of the form

$$\frac{1}{V} \langle T(\vec{k}) T^*(\vec{k}) \rangle P_{\text{null}}(\vec{k}') = P_{\text{null}}(\vec{k}) P_{\text{null}}(\vec{k}'), \quad (33)$$

for the null case. Finally, substituting Eqs. (32), (33), and (30), into Eq. (31), we get the following expression for the covariance

$$\langle \widehat{B}_0^{\vec{k}} \widehat{B}_0^{\vec{k}',*} \rangle = \frac{P_{\text{null}}^2(\vec{k}) \left( \delta_{\vec{k}, \vec{k}'} + \delta_{\vec{k}, -\vec{k}'} \right)}{\left( 2P_\delta(\vec{k}) \text{Re} \left[ G_0^*(\widehat{\mathbf{k}}) \frac{\partial G_0}{\partial B}(\widehat{\mathbf{k}}) \right] \right)^2}, \quad (34)$$

where we used reality of the temperature field ( $T(\vec{k}) = T^*(-\vec{k}')$ ), and the isotropy of space in the null-assumption case ( $G(\widehat{\mathbf{k}}) = G(-\widehat{\mathbf{k}})$ ). This covariance matrix is singular, and the only non-vanishing entries are those relating the same mode with itself (or to the same mode in the opposite direction). In this case, the usual expression for a minimum-variance estimator reduces to

$$\widehat{B}_0 = \frac{\sum_{\vec{k}} \frac{\widehat{B}_0^{\vec{k}}}{\sigma_k^2}}{\sum_{\vec{k}} \frac{1}{\sigma_k^2}}, \quad (35)$$

where  $\sigma_k^2 \equiv \langle \widehat{B}_0^{\vec{k}} \widehat{B}_0^{\vec{k}',*} \rangle$ , and the sums are restricted to a half of the available volume to avoid double-counting modes.

We can now proceed to combine estimates from all available modes with inverse-variance weights in order to obtain the optimal estimate. The final expression for the estimator is

$$\widehat{B}_0 = \frac{\sum_{\vec{k}} \frac{\frac{1}{V} T(\vec{k}) T^*(\vec{k}) - P_{\text{null}}(\vec{k})}{P_{\text{null}}^2(\vec{k})} 2P_\delta(k) \text{Re} \left[ G_0(\widehat{\mathbf{k}}) \frac{\partial G_0}{\partial B}(\widehat{\mathbf{k}}) \right]}{\sum_{\vec{k}} \left( \frac{2P_\delta(k) \text{Re} \left[ G_0(\widehat{\mathbf{k}}) \frac{\partial G_0}{\partial B}(\widehat{\mathbf{k}}) \right]}{P_{\text{null}}(\vec{k})} \right)^2}, \quad (36)$$

and its variance is given by

$$\sigma_{\widehat{B}_0}^{-2} = \sum_{\vec{k}} \left( \frac{2P_\delta(k) \text{Re} \left[ G_0^*(\widehat{\mathbf{k}}) \frac{\partial G_0}{\partial B}(\widehat{\mathbf{k}}) \right]}{G_0^2(\widehat{\mathbf{k}}) P_\delta(k) + P^N(\vec{k})} \right)^2, \quad (37)$$

where all the sums are restricted to one half of the plane.

## B. Stochastic field

We now derive a minimum-variance quadratic estimator for Fourier modes of a stochastic magnetic field. Note that in this Section we do *not* assume a particular model for its power spectrum. We use  $B_i$  to denote a component of  $\vec{B}$  along one of the three Cartesian-system axes, and  $\vec{x}$  to denote a position vector in physical space. We start with

$$T^S(\vec{x}) = T_0^S(\vec{x}) + B_i(\vec{x}) \frac{\partial T_0^S}{\partial B_i}(\vec{x}), \quad (38)$$

where the subscripts and superscripts have the same meaning as before. Note that the distinction from the uniform field case is that  $B$  (and its components) is now a function of  $\vec{x}$ . We then transition to Fourier space,

$$\begin{aligned} T^S(\vec{k}) &= T_0^S(\vec{k}) + \int d\vec{x} e^{-i\vec{k} \cdot \vec{x}} B_i(\vec{x}) \frac{\partial T_0^S}{\partial B_i}(\vec{x}) \\ &= T_0^S(\vec{k}) + \frac{1}{(2\pi)^3} \int d\vec{k}_1 B_i(\vec{k}_1) \frac{\partial T_0^S}{\partial B_i}(\vec{k} - \vec{k}_1), \end{aligned} \quad (39)$$

where  $k_1$  is the integration variable, and the last step used the convolution theorem.

In this case, the observable 2-point correlation function in Fourier space becomes

$$\begin{aligned} & \langle T(\vec{k}) T^*(\vec{k}') \rangle = P_{\text{null}}(\vec{k}) (2\pi)^3 \delta_D(\vec{k} - \vec{k}') \\ & + \left\langle T_0^*(\vec{k}') \frac{1}{(2\pi)^3} \int d\vec{k}_1 B_i(\vec{k}_1) \frac{\partial T_0}{\partial B_i}(\vec{k} - \vec{k}_1) \right\rangle \\ & + \left\langle T_0(\vec{k}) \frac{1}{(2\pi)^3} \int d\vec{k}_1 B_i^*(\vec{k}_1) \left( \frac{\partial T_0}{\partial B_i}(\vec{k}' - \vec{k}_1) \right)^* \right\rangle, \end{aligned} \quad (40)$$

to first order in  $B_i$ . Expanding this expression further and transitioning from Dirac to Kronecked delta in order to perform the integrals within the brackets, we get

$$\begin{aligned} & \langle T(\vec{k}) T^*(\vec{k}') \rangle = (2\pi)^3 \delta_D(\vec{k} - \vec{k}') P_{\text{null}}(\vec{k}) + B_i(\vec{k} - \vec{k}') \\ & \times \left[ P_\delta(k') G_0^*(\widehat{\mathbf{k}}') \frac{\partial G_0}{\partial B_i}(\widehat{\mathbf{k}}') - P_\delta(k) G_0(\widehat{\mathbf{k}}) \frac{\partial G_0^*}{\partial B_i}(\widehat{\mathbf{k}}) \right], \end{aligned} \quad (41)$$

where we also used the reality of the  $B_i$  field,  $B_i^*(-\vec{K}) = -B_i(\vec{K})$ . Now, if we wish to estimate  $B_i(\vec{K} \equiv \vec{k} - \vec{k}')$  from  $\vec{k}, \vec{k}'$  pair of modes, following an analogous procedure to that used in §IV A, we get

$$\hat{B}_i^{\vec{k}\vec{k}'}(\vec{K}) = \frac{T(\vec{k})T^*(\vec{k}')}{P_\delta(k')G_0^*(\hat{\mathbf{k}}')\frac{\partial G_0}{\partial B_i}(\hat{\mathbf{k}}') - P_\delta(k)G_0(\hat{\mathbf{k}})\frac{\partial G_0^*}{\partial B_i}(\hat{\mathbf{k}})}, \quad (42)$$

where we only focus on terms  $\vec{K} \neq 0$  ( $\vec{k} \neq \vec{k}'$ ). The variance of this estimator (evaluated under the null assumption) is

$$\langle \hat{B}_i^{\vec{k}\vec{k}'}(\vec{K}) (\hat{B}_i^{\vec{k}\vec{k}'}(\vec{K}'))^* \rangle = \frac{\langle T(\vec{k})T^*(\vec{k}')T^*(\vec{k})T(\vec{k}') \rangle}{\left( P_\delta(k')G_0^*(\hat{\mathbf{k}}')\frac{\partial G_0}{\partial B_i}(\hat{\mathbf{k}}') - P_\delta(k)G_0(\hat{\mathbf{k}})\frac{\partial G_0^*}{\partial B_i}(\hat{\mathbf{k}}) \right) \left( P_\delta(k')G_0(\hat{\mathbf{k}})\frac{\partial G_0^*}{\partial B_i}(\hat{\mathbf{k}}') - P_\delta(k)G_0^*(\hat{\mathbf{k}}')\frac{\partial G_0}{\partial B_i}(\hat{\mathbf{k}}) \right)}. \quad (43)$$

Finally, using Eqs. (42) and (43), we can derive the full estimator for the mode  $B_i(\vec{K})$ , in the usual way (by combining the individual  $\hat{B}_i^{\vec{k}\vec{k}'}(\vec{K})$  estimates with inverse-variance weights, and normalizing appropriately); as this

is a straightforward exercise, we will not present this equation here. The null-case measurement of the power spectrum of  $B_i$  is the variance of its estimator, and reads

$$(2\pi)^3 \delta_D(\vec{K} - \vec{K}') P_{B_i}^N(\vec{K}) \equiv \langle \hat{B}_i(\vec{K}) \hat{B}_i(\vec{K}')^* \rangle = \left( \sum_{\vec{k}} \frac{1}{2} \frac{\left| P_\delta(k')G_0^*(\hat{\mathbf{k}}')\frac{\partial G_0}{\partial B_i}(\hat{\mathbf{k}}') - P_\delta(k)G_0(\hat{\mathbf{k}})\frac{\partial G_0^*}{\partial B_i}(\hat{\mathbf{k}}) \right|^2}{V^2 \left( G_0^2(\hat{\mathbf{k}})P_\delta(k) + P^N(\vec{k}) \right) \left( G_0^2(\hat{\mathbf{k}}')P_\delta(k') + P^N(\vec{k}') \right)} \right)^{-1}, \quad (44)$$

with the restriction  $\vec{K} = \vec{k} - \vec{k}'$ , and where the factor of  $1/2$  serves to avoid double-counting mode pairs. As before,  $P^N$  is given by Eq. (13). If we limit ourselves to the diagonal terms only,  $\vec{K} = \vec{K}'$ , then the lhs of

the above expression becomes  $V P_{B_i}^N(\vec{K})$ . The resulting expression for the noise power spectrum is

$$P_{B_i}^N(\vec{K}) = \left( \frac{(2\pi)^3}{2V} \sum_{\vec{k}} \frac{\left| P_\delta(k')G_0^*(\hat{\mathbf{k}}')\frac{\partial G_0}{\partial B_i}(\hat{\mathbf{k}}') - P_\delta(k)G_0(\hat{\mathbf{k}})\frac{\partial G_0^*}{\partial B_i}(\hat{\mathbf{k}}) \right|^2}{\left( G_0^2(\hat{\mathbf{k}})P_\delta(k) + P^N(\vec{k}) \right) \left( G_0^2(\hat{\mathbf{k}}')P_\delta(k') + P^N(\vec{k}') \right)} \right)^{-1}, \quad (45)$$

Note that only the components of  $\vec{B}$  in the plane of the sky have an effect of the observed brightness temperature, and so the results derived in this Section hold only for those components. The noise in these two components is not correlated, and the noise in the direction along the line of sight can be considered infinite.

Finally, note that a similar type of estimator can be written down for the directions of the uniform magnetic field, and, in principle, used to recover the direction of the magnetic field in a certain patch of the sky. However, in this work we only focus on its magnitude.

## V. FISHER ANALYSIS

We now use the key results of §IV to discuss estimation of sensitivity of future observations to detecting magnetic fields in the IGM at high redshifts. We first discuss the case of a field uniform in the entire survey volume, starting with the unsaturated case, where the strength of  $\vec{B}$  classically produces less than 1 radian of precession at all redshifts of interest, and then move on to discussing detectability in the saturated case, where  $\vec{B}$  is a strong field in this sense. Finally, we discuss detectability of a stochastic magnetic field with a scale-independent power spectrum.

### A. Uniform field case

If an experiment measures the power spectrum of the redshifted 21-cm brightness temperature, its sensitivity  $\sigma_{B_0}$  to recovering  $B_0$  is given by the usual Fisher formula. For the case of a uniform field, where Eq. (20) holds, the sensitivity is given by

$$\begin{aligned}\sigma_{B_0}^{-2} &= \int dV_{\text{patch}}(z) \frac{d\vec{k}}{(2\pi)^3} \left( \frac{\frac{\partial P^S}{\partial B_0}(\vec{k})}{P^N(\vec{k}) + P_0^S(\vec{k})} \right)^2 \\ &= \int dV_{\text{patch}}(z) \frac{k^2 dk d\phi_k \sin \theta_k d\theta_k}{2(2\pi)^3} \\ &\quad \times \left( \frac{2P_\delta(k, z)G_0(\theta_k, \phi_k, z) \frac{\partial G_0}{\partial B}(\theta_k, \phi_k, z)}{P^N(k, \theta_k, z) + P_\delta(k, z)G_0^2(\theta_k, \phi_k, z)} \right)^2,\end{aligned}\quad (46)$$

where we transitioned from a sum over  $\vec{k}$  modes to an integral, using  $\sum_{\vec{k}} \rightarrow V \int d\vec{k}/(2\pi)^3$ . The integral is performed over  $V_{\text{patch}}$ , the (comoving) volume of the survey of angular size  $\Omega_{\text{survey}}$  (in steradians) at a given redshift,

$$dV_{\text{patch}} = \frac{c}{H(z)} \chi^2(z) \Omega_{\text{survey}} dz. \quad (47)$$

The integration limits are:  $\phi_k \in [0, 2\pi]$ ;  $\theta_k \in [0, \pi]$ ; and  $k \in [2\pi u_{\min}/(d_A \sin \theta_k), 2\pi u_{\max}/(d_A \sin \theta_k)]$ , where  $u_{\min, \max} = \frac{L_{\min, \max}}{\lambda}$  correspond to the maximum and minimum baseline  $L_{\min}$  and  $L_{\max}$ , respectively.

The integral in Eq. (46) is performed on a small, approximately flat, patch of the sky. If the survey area is big enough that the flat-sky approximation does not hold, the following geometric correction factor can be applied

$$P_{B_i}^N(\vec{K}) = \left( \frac{1}{2} \int k^2 dk \sin \theta_k d\theta_k d\phi_k \frac{\left| P_\delta(k') G_0^*(\hat{\mathbf{k}}') \frac{\partial G_0}{\partial B_i}(\hat{\mathbf{k}}') - P_\delta(k) G_0(\hat{\mathbf{k}}) \frac{\partial G_0^*}{\partial B_i}(\hat{\mathbf{k}}) \right|^2}{\left( G_0^2(\hat{\mathbf{k}}) P_\delta(k) + P^N(\vec{k}) \right) \left( G_0^2(\hat{\mathbf{k}}') P_\delta(k') + P^N(\vec{k}') \right)} \right)^{-1}, \quad (50)$$

with the condition  $\vec{k}' = \vec{K} - \vec{k}$ .

To simplify the calculation, in the following, we only focus on signal-to-noise ratio (SNR) for detecting a particular model of magnetic field power spectrum. Namely, we consider the case where most of the signal comes from the largest modes (smallest  $\vec{K}$ 's). In this (squeezed) limit,  $\vec{K} \ll \vec{k}$  and thus  $\vec{k} \approx \vec{k}'$ , such that the noise power spectrum of Eq. (50) becomes white noise (independent on  $\vec{K}$ ). If we further denote pixels with Greek indicies, and, as before, retain Roman indicies for components of

<sup>1</sup> This accounts for the change in the angle that a uniform magnetic field makes with a line of sight, as the line of sight moves through a large survey area.

1

$$\begin{aligned}\sigma_{B_0, \text{survey}}^{-2} &= \frac{\sigma_{B_0}^{-2}}{\Omega_{\text{patch}}} \int_0^{\theta_{\text{survey}}} \int_0^{2\pi} \cos^2 \theta d\theta d\phi \\ &= \frac{\sigma_{B_0}^{-2} \pi}{\Omega_{\text{patch}}} (\theta_{\text{survey}} + \cos \theta_{\text{survey}} \sin \theta_{\text{survey}}).\end{aligned}\quad (48)$$

Finally, let us now consider a field that is strong enough so as to produce precession by more than a radian in a lifetime of the excited state. This is the “saturated case”. The brightness-temperature power spectrum still captures the presence of the field in this case, but it loses sensitivity to recovering its exact magnitude. Sensitivity to distinguishing saturated case from zero magnetic field becomes a relevant quantity in this case.

We can write the signal power spectrum as a sum of the contributions from the case  $B_0 = 0$  and from the saturated case scenario of a very strong field (denoted as infinity),

$$P^S(\vec{k}) = (1 - \xi) P^S(\vec{k}, B = 0) + \xi P^S(\vec{k}, B \rightarrow \infty). \quad (49)$$

We can then perform the standard Fisher analysis, completely analogous to the unsaturated case, in order to make projections for sensitivity to measuring  $\xi$ , where  $\sigma_\xi$  gives a  $1\sigma$  sensitivity to *detecting* presence of a strong magnetic field.

### B. Stochastic field case

Let us now discuss the case of a stochastic field. Using Eq. (45), with a procedure analogous to the case of a uniform field, we get

$\vec{B}$ , then the pixel-noise variance for measuring a single mode  $\vec{K}$  of  $B_i$  component is  $\sigma_{B_i}^2 \equiv P_{B_i}^N(z)/V_{\text{voxel}}$ , where  $V_{\text{voxel}}$  is volume of a survey voxel (3d pixel). The model for the power spectrum is defined through

$$(2\pi)^3 \delta_D(\vec{K} - \vec{K}') P_{B_i B_j}(\vec{K}) = \langle B_i^*(\vec{K}) B_j(\vec{K}') \rangle, \quad (51)$$

which relates to the variance in the transverse component  $P_B(\vec{K})$  as

$$P_{B_i B_j}(\vec{K}) = (\delta_{ij} - \hat{K}_i \hat{K}_j) P_B(\vec{K}), \quad (52)$$

where  $\hat{K}_{i/j}$  is a unit vector along the direction of a  $B_{i/j}$  component. In this discussion, as a model example, we consider a scale-independent (SI) power spectrum, were

$$P_B(\vec{K}) = A_0^2 / K^3, \quad (53)$$



and the amplitude  $A_0$  is a free parameter in units of Gauss.

To compute SNR for measuring the amplitude of an arbitrary power-spectrum model in a given redshift slice  $z$ , we have to perform a sum over all voxels in the survey volume at that  $z$ . The general expression for SNR is

$$\text{SNR}^2 = \frac{1}{2} \text{Tr} (N^{-1} S N^{-1} S), \quad (54)$$

where  $S$  is the signal matrix,  $N$  is the noise matrix. In our case, these matrices are  $3N_{\text{voxels}} \times 3N_{\text{voxels}}$  (assuming there are  $N_{\text{voxels}}$  voxels in the entire survey, and that there are 3 components of  $\vec{B}$ ). In the null case, voxels are independent, and so the noise matrix is diagonal, and the signal is the 3d power spectrum of the vector field  $\vec{B}$ . For a single redshift slice, this evaluates to

$$\begin{aligned} \text{SNR}^2(z) &= \frac{1}{2} \sum_{i\alpha, j\beta} \frac{S_{i\alpha, j\beta}^2}{P_{B_i}^N(\vec{K}, z) P_{B_j}^N(\vec{K}, z)} V_{\text{voxel}}^2 \\ &= \frac{1}{2} \sum_{ij} \int d\vec{r}_\alpha \int d\vec{r}_\beta \frac{\langle B_i(\vec{r}_\alpha) B_j(\vec{r}_\beta) \rangle^2}{P_{B_i}^N(\vec{K}, z) P_{B_j}^N(\vec{K}, z)}, \end{aligned} \quad (55)$$

where  $\vec{r}_{\alpha/\beta}$  represents spatial position of a given voxel, and the expectation value on the rhs of the above equation relates to the model power spectrum. If homogeneity and isotropy are satisfied, the integrand should only depend on the separation vector  $\vec{s} \equiv \vec{r}_\beta - \vec{r}_\alpha$ , which gives<sup>2</sup>

$$\begin{aligned} \text{SNR}^2(z) &= \frac{1}{2} \sum_{ij} \frac{dV_{\text{patch}}}{(P_{B_i}^N(z))^2} \int d\vec{s} \langle B_i(\vec{r}_\beta - \vec{s}) B_j(\vec{r}_\beta) \rangle^2 \\ &= \frac{1}{2(2\pi)^3} \sum_{ij} \frac{dV_{\text{patch}}}{(P_{B_i}^N(z))^2} \int d\vec{K} \left( P_{B_i B_j}(\vec{K}) \right)^2, \end{aligned} \quad (56)$$

where  $dV_{\text{patch}}$  is the volume of a redshift-slice patch at  $z$ , given by Eq. (47). Substituting Eq. (53), and integrating over all  $z$ 's available in the survey,

$$\begin{aligned} \text{SNR}^2 &= \frac{A_0^4}{2(2\pi)^3} \int_{z_{\min}}^{z_{\max}} \frac{dV_{\text{patch}}}{(P_{B_i}^N(z))^2} \int_0^\pi \sin \theta d\theta \\ &\int_0^{2\pi} d\phi \int_{K_{\min}(z, \theta, \phi)}^{K_{\max}(z, \theta, \phi)} \frac{dK}{K^4} \sum_{ij \in \{xx, xy, yx, yy\}} (\delta_{ij} - \hat{K}_i \hat{K}_j)^2, \end{aligned} \quad (57)$$

where

$$\hat{K}_x = \sin \theta \sin \phi, \quad \hat{K}_y = \sin \theta \cos \phi. \quad (58)$$

The sum in the above expression reduces to

$$\sum_{ij \in \{xx, xy, yx, yy\}} (\delta_{ij} - \hat{K}_i \hat{K}_j)^2 = 2 - \sin^2 \theta (1 + \sin^2 \phi \cos^2 \phi). \quad (59)$$

<sup>2</sup> Note that in the last step we used  $\int d\vec{s} |f(\vec{s})|^2 = \int \frac{d\vec{K}}{(2\pi)^3} |\tilde{f}(\vec{K})|^2$ , for an arbitrary function  $f$  and its Fourier transform  $\tilde{f}$ .

Substituting this into Eq. (57), we get

$$\begin{aligned} \text{SNR}^2 &= \frac{A_0^4}{2(2\pi)^3} \int_{z_{\min}}^{z_{\max}} \frac{dV_{\text{patch}}}{(P_{B_i}^N(z))^2} \int_0^\pi d\theta \\ &\int_0^{2\pi} d\phi (2 - \sin^2 \theta (1 + \sin^2 \phi \cos^2 \phi)) \int_{K_{\min}(z, \theta, \phi)}^{K_{\max}(z, \theta, \phi)} \frac{dK}{K^4}. \end{aligned} \quad (60)$$

Finally, performing the integration over  $K, \theta, \phi$  analytically, for the FFTT case gives

$$\text{SNR}^2 = \frac{7A_0^4}{36\pi} \int_{z_{\min}}^{z_{\max}} \frac{dV_{\text{patch}}}{(P_{B_i}^N(z))^2} \left( \frac{1}{K_{\min}^3} - \frac{1}{K_{\max}^3} \right), \quad (61)$$

where  $P_{B_i}^N$  is given by Eq. (50); as before,  $K_{\min}$  is taken to correspond to the largest mode that fits a given survey volume,  $K_{\min} = 2\pi/d_A$ , and  $K_{\max} = \Delta L/\lambda(z)$  (note that the numerical value of  $K_{\max}$  makes very little difference in the total value of this integral). When the last expression is evaluated at  $A_0 = 1$ , it provides the inverse of a value of  $A_0$  detectable at  $1\sigma$  sensitivity with a given experiment.

## VI. RESULTS

We now proceed to numerically evaluate the sensitivity of a tomographic 21-cm survey to detecting magnetic fields during the pre-reionization epoch, using the formalism of previous two Sections. For the purposes of deriving numerical results, we only focus on one type of experimental setup—an array of closely-packed dipole antennas, such as the FFTT considered in §III C. The motivation for this choice is the fact that such configuration is known to maximize sensitivity of measurements based on the 2-point statistics [32], such as the one we propose in this work. For the parameters of this survey, we assume that a surface area of  $(\Delta L \text{ km})^2$  is covered in dipole antennas, and that the experiment observes  $\Omega_{\text{survey}} = 1\text{sr}$  of the sky for about 5 years.<sup>3</sup> For the sky temperature that enters the calculation of the noise power spectrum in Eq. (13), we assume a simple model of Galactic foregrounds from [34], where

$$T_{\text{sky}} = 60 \left( \frac{21}{100} (1+z) \right)^{2.55} \text{ [K]}. \quad (62)$$

Furthermore, we assume that the redshift range covered by the survey is  $z \in [15, 35]$ . Other ingredients entering the sensitivity calculation are the Lyman- $\alpha$  flux  $J_{\text{Ly}\alpha}(z)$ , and the spin and kinetic temperatures of the IGM; these

<sup>3</sup> The value used to evaluate Fisher formulas is actually 2 years. When corrected for the effect of Earth's rotation, and the fact that a given sky patch is above the horizon for only a fraction of a day, the effective observation time of 2 years translates to a (factor-of-a-few) longer wall-clock time.

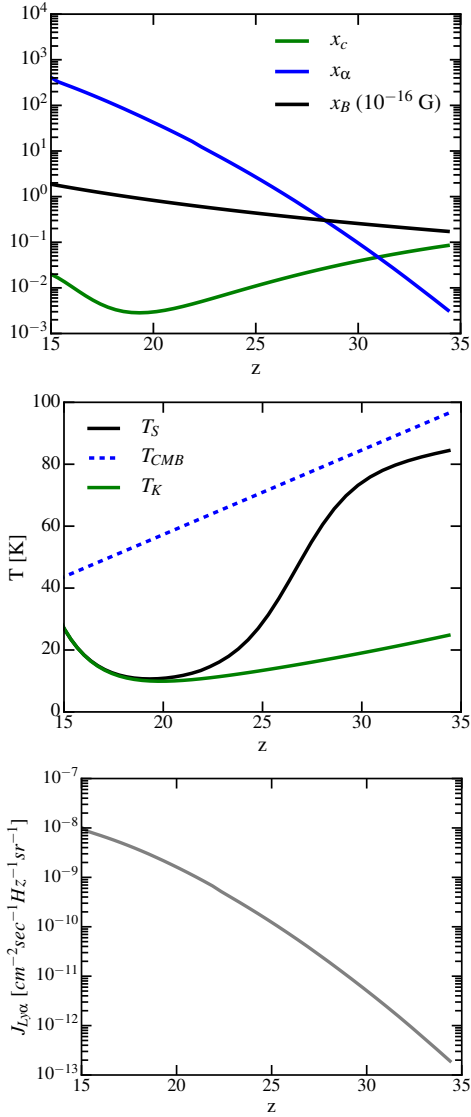


Figure 3. Inputs for sensitivity calculations: Lyman- $\alpha$  flux model, and the relevant spin- and kinetic- temperature models.

are obtained using 21CMFAST [35], for standard cosmology, and are shown in Figure 3. We checked that the variation in the x-ray heating rate within a factor of a few from the fiducial model does not make significant changes to the presented results.

Figures 4 and 5 show how the sensitivity changes as a function of the maximum baseline  $\Delta L$  (since different baselines may correspond to different stages of the experiment). Figure 4 shows  $1\sigma$  sensitivity to measuring parameter  $\xi$  of Eq. (49), that distinguishes amongst the zero magnetic field case and the case where the field is strong enough that the signal saturates (in the sense described in §II). This parameter is by definition bounded between the values of 0 and 1, where 0 represents the case of no magnetic field, and 1 represents the saturated case. From this Figure, we can see that, for example, a

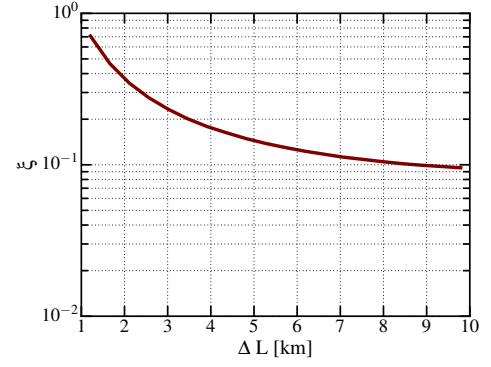


Figure 4. FFTT sensitivity to distinguishing saturated case from no magnetic field (upper panel), as a function of maximum array baseline, assuming a survey size of 1 sr, for survey duration of 2 years.

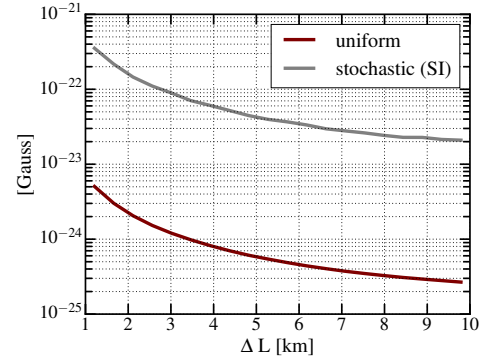


Figure 5. FFTT sensitivity to detecting a uniform and stochastic magnetic field (stochastic field is assumed to have a scale-independent (SI) power spectrum, and shown is the rms per  $\log K$ ,  $A_0/\pi$ ), as a function of maximum array baseline, assuming a survey size of 1 sr, for survey duration of 2 years.

little over a square kilometer of covarega area is necessary for a  $1\sigma$  detection of magnetic fields stronger than about  $10^{-21}$  Gauss comoving. While this size of a radio array is still futuristic in terms of the sheer number of antennas (compare to the SKA [27], for example), the number of mode measurements required for this measurement corresponds to the computational demands for the next-generation 21-cm cosmology experiment, and may thus be feasible in the coming couple of decades.

Figure 5 is obtained by evaluating the expressions of Eqs. (46) and (61), and shows sensitivity to measuring the scaled value of the magnetic field in the case of a uniform field (dark red line), and the sensitivity to measuring the amplitude of a particular model for a stochastic field (gray line)—the scale-independent (SI) power spectrum discussed in §V. While the numerical calculation behind this plot assumed that the brightness temperature is a linear function of the field strength, this assumption is not guaranteed to hold—it breaks in the saturation limit, as discussed in §II. In order to understand how the constraints (or, sensitivities) of Figure 5 compare

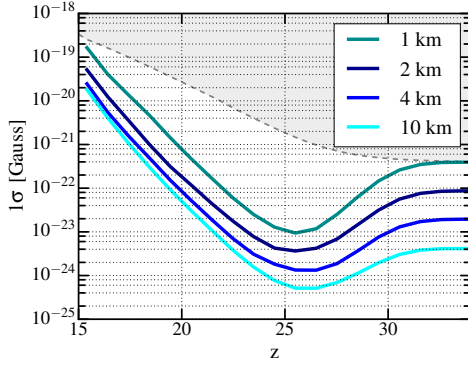


Figure 6. Saturation ceiling is shown as a shaded gray area, and integrand of Eq. (46) (inverse square root of it) is shown as a function of redshift, for several maximum baseline sizes. When the colored curves are below the saturation limit around their minima, the analysis assuming unsaturated regime is valid.

to the saturation “ceiling” at the redshifts we integrate over, we present a rough calculation of the saturation as a function of redshift, and compare it to the values of the  $z$ -dependent integrands of Eq. (46). From this Figure, we can see that only above the coverage of about  $16\text{km}^2$  are we able to actually measure the exact value of the amplitude of the magnetic field power spectrum.

## VII. CONCLUSIONS

In Paper I of this series, we proposed a new method to detect extremely weak magnetic fields in the IGM during the Dark Ages, using future 21-cm tomography experiments. In this paper, Paper II, we investigated sensitivity of future radio arrays using this method. We developed minimum-variance-estimator formalism that uses 2-point correlation function of the 21-cm brightness temperature to detect and measure magnetic fields in pre-reionization epoch.

Our results imply that the next-stage array with a little over a square kilometer of area covered in dipole antennas in a tightly-packed configuration, observing redshifts from 15 to 35, can in principle reach the sensitivity to detect magnetic fields on the order of  $10^{-21}$  Gauss comoving. However, disentangling the exact spectral shape of a stochastic field is more challenging, and can only be expected in the futuristic scenarios where arrays grow to a size of tens of square kilometers in coverage area. In this analysis, we took into account the noise arising from the presence of the large Galactic foreground signal, but we ignored more subtle effects such as, for example, frequency dependence of the beams, etc., calculation of which would be necessary to create figures of merit for future experiments.

At the end, we emphasize again that the main limitation to sensitivity of this method to measuring magnetic fields at high redshifts is a mere fact that it is based on a

two-scattering process—as soon as quality of the 21-cm statistics reaches the levels necessary to probe second-order processes, the effect we focused on in this series of papers will immediately open up an “*in situ*” way to trace miniscule (and possibly primordial) magnetic fields with unprecedented precision.

## ACKNOWLEDGMENTS

VG gratefully acknowledges the support from the W. M. Keck Foundation Fund. Illustrations in Figure 2 made use of HEALPix [36] software package<sup>4</sup>.

## Appendix A: Visibility-variance derivation

Here we derive the variance of the visibility for an interferometric array of two antennas separated by a baseline  $\vec{b} = (b_x, b_y)$ , each with an effective collecting area  $A_e$ , observing a single element in  $uv$  plane for time duration  $t_1$ , in the total bandwidth  $\Delta\nu = \nu_{\text{max}} - \nu_{\text{min}}$ . This setup is shown in Figure 7. Note that modes with frequencies that differ by less than  $1/t_1$  cannot be distinguished in observation time  $t_1$ , and modes with frequencies in each interval of size  $1/t_1$  are “collapsed” into a discrete mode with  $\nu_n = n/t_1$ , where  $n \in \mathbb{Z}$ . Thus, the number of measured (discrete) frequencies is  $N_\nu = t_1 \Delta\nu$ .

Electric field induced in a single antenna is

$$E(t) = \sum_n^{N_\nu} \tilde{E}(\nu_n) e^{2\pi i \nu_n t}, \quad (\text{A1})$$

while the quantity an interferometer measures is the correlation coefficient between the electric field in one,  $E_i$ , and the electric field in the other antenna,  $E_j$ , as a function of frequency,

$$\rho_{ij}(\nu) \equiv \frac{\langle \tilde{E}_i^*(\nu) \tilde{E}_j(\nu) \rangle}{\sqrt{\langle |\tilde{E}_i(\nu)|^2 \rangle \langle |\tilde{E}_j(\nu)|^2 \rangle}}. \quad (\text{A2})$$

Let us now assume that

$$\langle \tilde{E}_i^*(\nu_n) \tilde{E}_j(\nu_m) \rangle = \sigma(\nu)^2 \delta_{mn}, \quad (\text{A3})$$

In the following, for clarity, we will omit writing the explicit dependence on  $\nu$ . The real (or imaginary) part of  $\rho$  has the following variance

$$\begin{aligned} & \text{var}(\text{Re}[\rho_{ij}]) \\ &= \frac{1}{(2\sigma^2)^2} \text{var}(\langle \text{Re}[\tilde{E}_i] \text{Re}[\tilde{E}_j] + \text{Im}[\tilde{E}_i] \text{Im}[\tilde{E}_j] \rangle) \\ &= \frac{2\sigma^2\sigma^2}{(2\sigma^2)^2} = \frac{1}{2N_\nu} = \frac{1}{2t_1\Delta\nu}. \end{aligned} \quad (\text{A4})$$

<sup>4</sup> <http://healpix.sf.net>; <https://github.com/healpy/healpy>

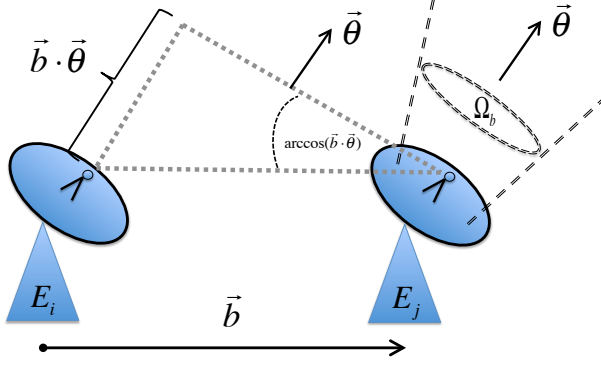


Figure 7. Two-antennae interferometer.

Before continuing, let us take a brief digression to show that the above formula implicitly assumes that the electric fields in the two antennas  $\tilde{E}_i$  and  $\tilde{E}_j$  have a very weak correlation,  $\rho \ll 1$ . Namely, suppose  $x$  and  $y$  are random Gaussian variables with zero mean values, where  $\text{var}(x) \equiv \langle (x - \langle x \rangle)^2 \rangle = \langle x^2 \rangle - \langle x \rangle^2 = \langle x^2 \rangle$ , and similarly for  $y$ , and their correlation coefficient is  $\rho \equiv \frac{\langle xy \rangle}{\sqrt{\langle x^2 \rangle \langle y^2 \rangle}}$ . In this case, the following is true

$$\begin{aligned} \text{var}(xy) &= \langle x^2 y^2 \rangle - \langle xy \rangle^2 = \langle x^2 \rangle \langle y^2 \rangle + \langle xy \rangle^2 \\ &= \langle x^2 \rangle \langle y^2 \rangle + \rho^2 \langle x^2 \rangle \langle y^2 \rangle = \text{var}(x) \text{var}(y) (1 + \rho^2), \end{aligned} \quad (\text{A5})$$

so that when  $\rho$  is small  $\text{var}(xy) = \text{var}(x) \text{var}(y)$ , which was assumed in the first equality of Eq. (A4).

Resuming the derivation, if different frequencies are uncorrelated, the result of Eq. (A4) implies

$$\langle |\rho_{ij}(\nu)|^2 \rangle = \frac{1}{t_1 \Delta \nu}. \quad (\text{A6})$$

The final step in this derivation requires the relation between intensity in the sky  $\mathcal{I}(\theta_x, \theta_y, \nu)$  (within the beam of the solid angle  $\Omega_b$ , centered on the direction  $(\theta_x, \theta_y)$ ) and the electric fields measured in the two antennas,

$$\begin{aligned} \langle \tilde{E}_i^*(\nu) \tilde{E}_j(\nu) \rangle &\propto \int_{\Omega_b} d\theta_x d\theta_y \mathcal{I}(\theta_x, \theta_y, \nu) \\ &\times e^{i \frac{2\pi \nu}{c} (b_x \theta_x + b_y \theta_y)} R(\theta_x, \theta_y), \end{aligned} \quad (\text{A7})$$

where  $R(\theta_x, \theta_y)$  is the antenna response function (the shape of the beam in the sky), which we will assume to be unity. Furthermore,  $\frac{2\pi \nu}{c} (b_x \theta_x + b_y \theta_y) \equiv 2\pi (u \theta_x + v \theta_y)$  is the phase delay between two antennae (position in the  $uv$  plane measures the phase lag between the two dishes in wavelengths). The coefficient of proportionality in the above equation is set by various instrumental parameters, and is not relevant for our purposes. From Eq. (A2), it follows

$$\rho_{ij}(\nu) = \frac{\int_{\Omega_b} d\theta_x d\theta_y \mathcal{I}(\theta_x, \theta_y, \nu) e^{2\pi i (u \theta_x + v \theta_y)}}{\int_{\Omega_b} d\theta_x d\theta_y \mathcal{I}(\theta_x, \theta_y, \nu)}, \quad (\text{A8})$$

where the denominator in the above formula approximately integrates to (for a small beam)

$$\int_{\Omega_b} d\theta_x d\theta_y \mathcal{I}(\theta_x, \theta_y, \nu) \approx \Omega_b \mathcal{I}(\theta_x, \theta_y, \nu). \quad (\text{A9})$$

We can now use the approximate expression for the resolution of a single dish,

$$\Omega_b = \frac{\lambda^2}{A_e}, \quad (\text{A10})$$

the Rayleigh-Jeans law (or the definition of the brightness temperature),

$$\mathcal{I}(\theta_x, \theta_y, \nu) = \frac{2k_B T_{\text{sky}}}{\lambda^2}, \quad (\text{A11})$$

and note that the numerator in Eq. (A8) matches the definition of visibility from Eq. (6) to get

$$\rho_{ij}(\nu) = \frac{A_e}{2k_B T_{\text{sky}}} V(u, v, \theta_\nu), \quad (\text{A12})$$

Combining the above expression and Eq. (A6), we get the final result of this derivation,

$$\langle |V(u, v, \theta_\nu)|^2 \rangle = \left( \frac{2k_B T_{\text{sky}}}{A_e \sqrt{t_1 \Delta \nu}} \right)^2 \delta(u - u') \delta(v - v') \delta_{\theta_\nu, \theta_{\nu'}}, \quad (\text{A13})$$

where  $V$  is a complex Gaussian variable, centered at zero, and uncorrelated for different values of its arguments.

It should be noted at the end that we were calculating the contribution to the visibility from the noise only (the system + the foregrounds in the absence of a signal), so we used system temperature for brightness temperature (this could contain the signal from foregrounds and from the instrument). In case we want to repeat the computation in the presence of a signal,  $T_{\text{sky}}$  should instead be the sum of the signal and the noise temperatures.

[1] R. Durrer and A. Neronov, *Astron. and Astrophys. Review* **21**, 62 (2013), arXiv:1303.7121 [astro-ph.CO].

[2] J. P. Vallee, *New Astronomy Reviews* **48**, 763 (2004).  
[3] A. Neronov and I. Vovk, *Science* **328**, 73 (2010),

- arXiv:1006.3504 [astro-ph.HE].
- [4] R. Wielebinski, in *Cosmic Magnetic Fields*, Lecture Notes in Physics, Berlin Springer Verlag, Vol. 664, edited by R. Wielebinski and R. Beck (2005) p. 89.
  - [5] R. Beck, *Space Science Reviews* **166**, 215 (2012).
  - [6] K. Park, E. G. Blackman, and K. Subramanian, *Phys. Rev. E* **87**, 053110 (2013), arXiv:1305.2080 [physics.plasm-ph].
  - [7] S. Naoz and R. Narayan, *Physical Review Letters* **111**, 051303 (2013), arXiv:1304.5792 [astro-ph.CO].
  - [8] S. Naoz and R. Narayan, *Physical Review Letters* **111**, 051303 (2013), arXiv:1304.5792 [astro-ph.CO].
  - [9] L. M. Widrow, D. Ryu, D. R. G. Schleicher, K. Subramanian, C. G. Tsagas, and R. A. Treumann, *Space Science Reviews* **166**, 37 (2012), arXiv:1109.4052 [astro-ph.CO].
  - [10] T. Kobayashi, *Journal of Cosmology and Astroparticle Physics* **5**, 040 (2014), arXiv:1403.5168.
  - [11] D. G. Yamazaki, K. Ichiki, T. Kajino, and G. J. Mathews, *Advances in Astronomy* **2010** (2010), arXiv:1112.4922 [astro-ph.CO].
  - [12] P. Blasi, S. Burles, and A. V. Olinto, *Astrophysical Journal, Letters* **514**, L79 (1999), astro-ph/9812487.
  - [13] F. Tavecchio, G. Ghisellini, L. Foschini, G. Bonnoli, G. Ghirlanda, and P. Coppi, *MNRAS* **406**, L70 (2010), arXiv:1004.1329 [astro-ph.CO].
  - [14] K. Dolag, M. Kachelriess, S. Ostapchenko, and R. Tomàs, *Astrophysical Journal, Letters* **727**, L4 (2011), arXiv:1009.1782 [astro-ph.HE].
  - [15] K. E. Kunze and E. Komatsu, *Journal of Cosmology and Astroparticle Physics* **1**, 009 (2014), arXiv:1309.7994 [astro-ph.CO].
  - [16] T. Kahnashvili, Y. Maravin, A. Natarajan, N. Battaglia, and A. G. Tevzadze, *Astrophys. J.* **770**, 47 (2013), arXiv:1211.2769 [astro-ph.CO].
  - [17] M. Shiraishi, H. Tashiro, and K. Ichiki, *Phys. Rev. D* **89**, 103522 (2014), arXiv:1403.2608.
  - [18] H. Tashiro and N. Sugiyama, *Mon. Not. R. Astron. Soc.* **372**, 1060 (2006), astro-ph/0607169.
  - [19] D. R. G. Schleicher, R. Banerjee, and R. S. Klessen, *Astrophys. J.* **692**, 236 (2009), arXiv:0808.1461.
  - [20] Planck Collaboration, P. A. R. Ade, N. Aghanim, M. Arnaud, F. Arroja, M. Ashdown, J. Aumont, C. Baccigalupi, M. Ballardini, A. J. Banday, and et al., ArXiv e-prints (2015), arXiv:1502.01594.
  - [21] T. Venumadhav, A. Oklopčic, V. Gluscevic, A. Mishra, and C. M. Hirata, ArXiv e-prints (2014), arXiv:1410.2250.
  - [22] P. Madau, A. Meiksin, and M. J. Rees, *Astrophys. J.* **475**, 429 (1997), astro-ph/9608010.
  - [23] A. Loeb and M. Zaldarriaga, *Physical Review Letters* **92**, 211301 (2004), astro-ph/0312134.
  - [24] L. J. Greenhill and G. Bernardi, ArXiv e-prints (2012), arXiv:1201.1700 [astro-ph.CO].
  - [25] J. D. Bowman, M. F. Morales, J. N. Hewitt, and MWA Collaboration, in *American Astronomical Society Meeting Abstracts #218* (2011) p. 132.06.
  - [26] A. R. Parsons, A. Liu, J. E. Aguirre, Z. S. Ali, R. F. Bradley, C. L. Carilli, D. R. DeBoer, M. R. Dexter, N. E. Gugliucci, D. C. Jacobs, P. Klima, D. H. E. MacMahon, J. R. Manley, D. F. Moore, J. C. Pober, I. I. Stefan, and W. P. Walbrugh, *Astrophys. J.* **788**, 106 (2014), arXiv:1304.4991.
  - [27] C. L. Carilli, ArXiv e-prints (2008), arXiv:0802.1727.
  - [28] K. Vanderlinde and Chime Collaboration, in *Exascale Radio Astronomy* (2014) p. 10102.
  - [29] D. R. DeBoer and HERA, in *American Astronomical Society Meeting Abstracts*, American Astronomical Society Meeting Abstracts, Vol. 225 (2015) p. 328.03.
  - [30] H. Yan and A. Lazarian, *Astrophys. J.* **677**, 1401 (2008), arXiv:0711.0926.
  - [31] H. Yan and A. Lazarian, *J. Quant. Spec. Rad. Trans.* **113**, 1409 (2012), arXiv:1203.5571 [astro-ph.GA].
  - [32] M. Tegmark and M. Zaldarriaga, *Phys. Rev. D* **79**, 083530 (2009), arXiv:0805.4414.
  - [33] T. Okamoto and W. Hu, *Phys. Rev. D* **67**, 083002 (2003), astro-ph/0301031.
  - [34] Y. Mao, M. Tegmark, M. McQuinn, M. Zaldarriaga, and O. Zahn, *Phys. Rev. D* **78**, 023529 (2008), arXiv:0802.1710.
  - [35] A. Mesinger, S. Furlanetto, and R. Cen, *Mon. Not. R. Astron. Soc.* **411**, 955 (2011), arXiv:1003.3878.
  - [36] K. M. Górski, E. Hivon, A. J. Banday, B. D. Wandelt, F. K. Hansen, M. Reinecke, and M. Bartelmann, *Astrophys. J.* **622**, 759 (2005), astro-ph/0409513.